Distributed Sliding Mode Control for Nonlinear Heterogeneous Platoon Systems With Positive Definite Topologies

Yujia Wu, *Student Member, IEEE,* Shengbo Eben Li, *Senior Member, IEEE,* Jorge Cortés, *Fellow, IEEE,* and Kameshwar Poolla, *Fellow, IEEE*

***Abstract*—This paper is concerned with the distributed control of vehicle platoons. The dynamics of each vehicle are nonlinear and heterogeneous. The control objective is to regulate vehicles to travel at a common speed while maintaining desired inter-vehicle gaps. The information flow topology dictates the pattern of communication between vehicles in the platoon. This information is essential to effective platoon control, and therefore plays a central role in affecting the design and performance of platoon control strategies. Our key contribution is a unified distributed control framework that explicitly incorporates and supports a diversity of information flow topologies. Specifically, we propose a distributed sliding mode control (DSMC) framework for a class of generic topologies. The DSMC constructs the topological sliding surface and reaching law via a so-called "topologically structured function". The control law obtained by matching the topological sliding surface and topological reaching law is naturally distributed. The Lyapunov stability analysis is carried out for the closed-loop system in the sense of Filippov to cope with the discontinuity originated from switching terms. Moreover, a trade-off between tracking precision and chattering elimination is discussed with a continuous approximation of the switching control law. The effectiveness of the DSMC for platoons is verified under four different topologies through numerical simulation.**

I. Introduction

The platooning of connected and automated vehicles is attracting increasing attention due to its potential in increasing traffic throughput and infrastructure utilization, enhancing driving safety, and reducing fuel consumption. The objective of the platoon control system is to regulate vehicles to travel at a common speed while maintaining desired inter-vehicle gaps [1], [2].

A. Related Work

Platooning was first proposed in the well-known PATH project [3], where linear control strategies were designed and implemented based on linearized vehicle models. Importantly, this work focused on a fixed communication topology of information exchange between vehicles. Following this, diverse aspects of platoon control have been explored, including control architecture, platoon modeling, spacing policy, controller synthesis, and performance requirements. Some representative examples of research include selection of spacing policies [4], string stability [5], scalability [6], direct consideration of powertrain dynamics [7], dynamic homogeneity and heterogeneity [8]. A recent review on platoon control can be found in [9].

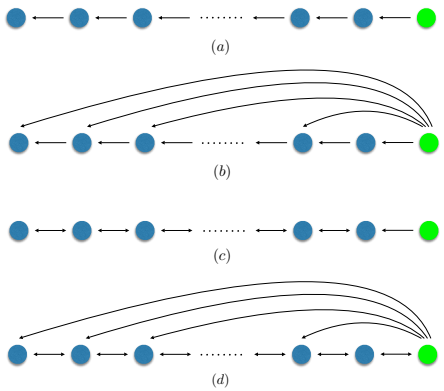

Fig. 1. Common topologies: (a) predecessor following topology, (b) leader-predecessor following topology, (c) bidirectional topology, (d) leader-bidirectional topology.

The information exchange topology plays a key role in the design of platoon control systems [9]. Much of the early research on platoon control focused on radar-based sensing systems, where information topologies were limited to predecessor following topology [10], [11]. The topology is shown in Figure 1 (a), where directed links denote information exchange. With the rapid adoption of vehicle-to-vehicle (V2V) communications [12], a variety of new information topologies can be supported, which offer the promise of high performance and robust platoon control. These include leader-predecessor following topology [5], bidirectional topology [13] and leader-bidirectional topologies (see Figure 1).

Under this diversity of possible information topologies, new control challenges emerge, particular when systematically considering nonlinear vehicle dynamics, communication delay and topology switching. As a result, *it is advantageous to view the vehicle platoon as a multi-agent system, and to employ a networked control perspective to design distributed controllers* [6]. This has led to new advanced control methods for platoon control. For instance, a mistuning-based control method is introduced to improve stability margin of vehicle platoons

Corresponding author: Shengbo Eben Li.

* Y. Wu and K. Poolla are with Department of Mechanical Engineering, University of California, Berkeley, CA, 94720. Email: {yujia.wu, poolla}@berkeley.edu.

† S. Li is with Department of Automotive Engineering, State Key Lab of Automotive Safety and Energy, Tsinghua University, Beijing, 100084, China. Email: lishbo@tsinghua.edu.cn, lisb04@gmail.com

‡ J. Cortés is with Department of Mechanical and Aerospace Engineering, University of California, San Diego, California, 92093. Email: cortes@ucsd.edu.

[14]; $\mathcal{H}_\infty$ controllers are developed to satisfy string stability explicitly [15]; general linear control method is proposed for both fixed and switching topologies [16].

Sliding mode control (SMC) is a promising method to handle nonlinear dynamics, actuator constraints, and information topology diversity. The pioneering work of SMC research on platoon control was conducted by Swaroop and Hedrick (1996) under a fixed leader-predecessor following topology. Here, each following vehicle can access the position, velocity and acceleration information of both the lead vehicle and the preceding vehicle [5]. This work was the first to introduce and analyze the key notion of string stability of interconnected nonlinear systems. Under this information topology, Liu *et al.* (2001) explore the effects of network communication delays on the stability of the sliding-mode-controlled platoon system [17]. This research studies the effects of preceding-vehicle information delay and lead-vehicle information delay on string stability. Lee and Kim (2002) used fuzzy-sliding mode control for platoons with leader-predecessor following topology to address nonlinear vehicle dynamics and time-varying parametric uncertainty [18]. The fuzzy SMC controller generate throttle and brake commands without requiring high-fidelity vehicle models. For the predecessor-following topology, Ferrara (2009) designed a sliding mode controller for each vehicle in a platoon to track its preceding vehicle under a constant time-headway spacing policy [11]. Kwon and Chwa (2014) extended coupled sliding mode control to bidirectional topology where the preceding vehicle information is used in the sliding surface design [13]. Similar controller structures were used in [19] to integrate tracking errors into the sliding surface design, and to overcome bounded disturbances under different kinds of spacing policies.

The main shortcoming of existing research on SMC for vehicle platoons is that they are dedicated to *fixed* information topologies: leader-predecessor following topology in [5], [20], [17], and [18]; predecessor following topology in [10] and [11]; bidirectional topology in [13] and [19]. However, in a practical context, information topologies can vary as platoons are formed, or can change as topologies switch. This paper focuses on sliding mode control design for vehicle platoons that is agnostic to the dynamic nature of the information topology.

B. Our Contributions

This paper presents a distributed sliding mode control (DSMC) design framework for nonlinear heterogeneous vehicular platoons with a class of generic topologies. Taking a multi-agent perspective, we propose a new "topologically structured function" that is used to construct the topological sliding surface and reaching law. This design results naturally in a distributed control architecture. The distributed control law is obtained by properly matching the topological sliding surface and topological reaching law. The closed-loop stability is proved in the sense of Filippov to cope with the discontinuity originated from switching terms.

The remainder of this paper is organized as follows. The platoon control problem is formulated in Section II, design of DSMC is explored in Section III, stability results are presented in Section IV, robust performance of DSMC is analyzed in Section V and simulation studies are offered in Section VI. We draw conclusions and suggest future research problems in Section VII.

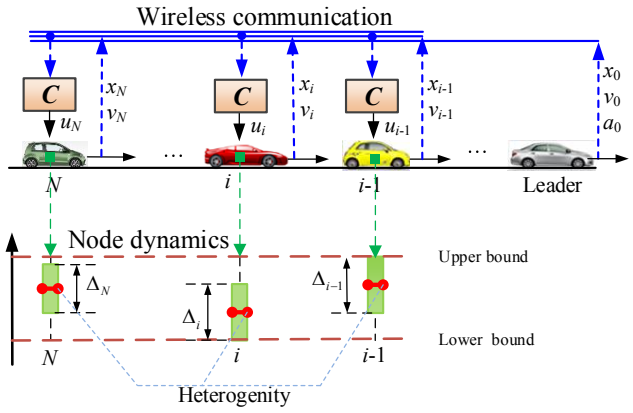

Fig. 2. Platoon : (a) vehicle dynamics, (b) information flow topology, (c) distributed controller, (d) geometry formation [6]

C. Notation

For a set M, its closure is written $\overline{M}$. The smallest convex set containing M (i.e., its convex hull) is denoted by co$M$. Equivalently, co$M$ is the set of all convex combination of points drawn from M. The set of positive real numbers is denoted as $\mathbb{R}^+$. For a function f, define $f(M)$ to be the image of M under f. For the affine function $f(x) = Ax + b$, where $A \in \mathbb{R}^{m\times n}$, we write $f(M) = AM + b$. If M is closed and bounded (i.e., compact), co$(AM + b) = A$co$M + b$.

For a symmetric matrix A, the maximum and minimum eigenvalues are denoted by $\lambda_{\max}(A)$ and $\lambda_{\min}(A)$, respectively. If A is positive definite, the square root of the matrix is denoted by $A^{\frac{1}{2}}$, which is also symmetric and positive definite. For a vector $x = [x_1, x_2, \cdots, x_n]^\top \in \mathbb{R}^n$, define $\mathrm{sgn}(x)$ as

$$\mathrm{sgn}(x) = [\mathrm{sgn}(x_1), \mathrm{sgn}(x_2), \cdots, \mathrm{sgn}(x_n)]^\top,$$

where

$$\mathrm{sgn}(x_i) = \begin{cases} -1, & x_i < 0, \\ 0, & x_i = 0, \\ 1, & x_i > 0. \end{cases} \quad \text{for } i \in \{1, \cdots, n\}.$$

II. Platoon Control Problem Formulation

A vehicle platoon is a multi-agent system as shown in Fig. 2. We refer to the vehicles that comprise the platoon as nodes. From a network control perspective, a platoon has four main components: node dynamics, distributed controllers, information flow topology, and formation geometry [9]. The node dynamics describe the behavior of each vehicle; the information flow topology defines how nodes exchange information with each other; the distributed controller implements feedback control algorithms for each vehicle; and the formation geometry defines the desired distance between any two successive vehicles.

The platoon contains a virtual leader, denoted by 0, and N following vehicles, denoted by $i \in \mathcal{N} \triangleq \{1, \ldots, N\}$. The displacement and velocity of the virtual leader are denoted by x_0 and v_0, respectively. We assume only a subset of vehicles have access to the leader's information. The stability analyses are carried out under two cases: (a) $\dot{v}_0$ is zero (Section IV), and (b) $\dot{v}_0 = \delta_0(t)$ is nonzero, unknown and bounded (Section V). The convergence to the equilibrium is analyzed in case (a) in the sense of Lyapunov stability, and the Input-to-State stability (ISS) is used in case (b) to demonstrate the disturbance attenuation performance of the platoon system.

The desired distance between two neighboring vehicles is assumed to be a constant $d \in \mathbb{R}^+$. The desired position for vehicle i is then

$$x_{i,des}(t) = x_0(t) - i \cdot d.$$

The purpose of platoon control is to ensure all the vehicles run at a harmonized speed while maintaining the desired inter-vehicle spaces.

A. Model for Information Flow Topology

The information exchange between the followers is assumed to be bidirectional, and its topology is described by an undirected graph $G = \{V, E\}$, in which V is the node set, and $E \subseteq V \times V$ is the edge set. The connectivity of graph G is represented by its adjacency matrix $\mathcal{A}$ defined as $\mathcal{A} = [a_{ij}] \in \mathbb{R}^{N\times N}$ and

$$\begin{cases} a_{ij} = 1, & (j,\, i) \in E, \\ a_{ij} = 0, & (j,\, i) \notin E, \end{cases} \quad i,\, j \in \mathcal{N}$$

where $(j,\, i) \in E$ means there is a edge from node j to node i, i.e., node i receives the information of j. It is assumed that there are no self-loops, i.e., $a_{ii} = 0$, $i \in \mathcal{N}$. The Laplacian matrix $\mathcal{L} = [l_{ij}] \in \mathbb{R}^{N\times N}$ is then defined as:

$$l_{ij} = \begin{cases} -a_{ij}, & i \neq j, \\ \sum\limits_{k=1,\, k\neq i}^{N} a_{ik}, & i = j, \end{cases} \quad i,\, j \in \mathcal{N}.$$

Since G is undirected, both $\mathcal{A}$ and $\mathcal{L}$ are symmetric. The neighbor set of node i is denoted by $\mathbb{N}_i = \{j | a_{ij} = 1, j \in \mathcal{N}\}$. G is connected if there is a path between any two vertices, otherwise, G is disconnected. A tree is an undirected graph in which any two vertices are connected by exactly one path. A spanning tree T of an undirected graph G is subgraph of G which is a tree and includes all of the vertices of G. If all of the edges of G are also edges of a spanning tree T of G, then G is a tree, identical to T.

We assume the leader can only send information, the connectivity between the leader and followers are directed, thus represented by directed edges. The pinning matrix $\mathcal{P}$ represents the direct connectivity between nodes and the leader. It is defined as

$$\mathcal{P} = \text{diag}\{p_1,\, p_2,\, \ldots, p_N\},$$

where $p_i = 1$ if there is an edge from leader to node i, and $p_i = 0$ otherwise.

Assumption 1: (*Positive definite assumption*) We assume that G contains a spanning tree, and there exists at least one edge from the leader to one of the followers.

Lemma 1: If the information flow topology of a platoon system satisfies Assumption 1, $\mathcal{L} + \mathcal{P}$ is positive definite.

Proof: See appendix B. ■

B. Nonlinear Model for Node Dynamics

The vehicle longitudinal dynamics are nonlinear, which are composed of engine, drive line, brake systems, aerodynamics drag, tire friction, rolling resistance, gravitational forces, *etc*. To strike a balance between accuracy and conciseness, we assume that: (1) the vehicle body is rigid and left-right symmetric, the vehicle length is assumed to be zero; (2) the platoon is on a flat and dry-asphalt road, and the tire slip in the longitudinal direction is neglected; (3) the driving and braking torques are integrated into one control input [21]. For a heterogeneous vehicle platoon, the i-th node dynamics are described by a nonlinear model:

$$\dot{x}_i(t) = v_i(t), \tag{1}$$

$$\dot{v}_i(t) = \frac{1}{m_i}\left(\eta_i \frac{T_i(t)}{R_i} - C_{A,i} v_i^2(t)\right) - gf, \tag{2}$$

where $x_i(t)$ and $v_i(t)$ are position and velocity, respectively; $T_i(t)$ is the control input, representing the driving/braking torque; m_i is the mass of vehicle; η_i is the mechanical efficiency of the driveline; R_i is the radius of wheel; $C_{A,i}$ is the coefficient of aerodynamic drag; g is the acceleration due to gravity; and f is the coefficient of rolling resistance.

III. DSMC for Nonlinear Heterogeneous Platoon

Our Distributed Sliding Mode Control design is composed of two parts: (a) the topological sliding surface selection, and (b) the topological reaching law design. Both the sliding surface and reaching law share a common structure defined by the topological structured function, which we introduce next.

Definition 1: (Topologically structured function) The topological structured function $f_i^{TS} : \mathbb{R}^N \to \mathbb{R}$ for node i is defined as

$$f_i^{TS}(Z) \triangleq \sum_{j=1, j\neq i}^{N} a_{ij}(z_i - z_j) + p_i z_i,$$

where $Z = [z_1,\, z_2,\, \ldots,\, z_N]^\top \in \mathbb{R}^N$, a_{ij} is the $(i,j)^{\text{th}}$ entry of the adjacency matrix, and p_i is the i-th element of the pinning matrix. In vector form, $F^{TS} : \mathbb{R}^N \to \mathbb{R}^N$,

$$\begin{aligned} F^{TS}(Z) \triangleq & [f_1^{TS}(Z),\, f_2^{TS}(Z),\, \ldots,\, f_N^{TS}(Z)]^\top \\ = & (\mathcal{L} + \mathcal{P})Z. \end{aligned}$$

A. Design of topological sliding surface

The tracking error of i-th vehicle is defined as

$$e_i \triangleq x_i - x_{i,des}.$$

Define an intermediate error Δ_i,

$$\Delta_i \triangleq \dot{e}_i + \rho e_i, \tag{3}$$

where $\rho \in \mathbb{R}^+$ is a tuning parameter. This parameter determines the converging rate of tracking error once the intermediate error equals zero. The intermediate error vector is defined as

$$\overline{\Delta} \triangleq [\Delta_1, \Delta_2, \ldots, \Delta_N]^\top.$$

We define the individual sliding variable for node i as

$$s_i \triangleq f_i^{TS}(\overline{\Delta}).$$

The sliding variable array of the platoon is then

$$S = \begin{bmatrix} s_1 \\ s_2 \\ \vdots \\ s_N \end{bmatrix} = (\mathcal{L} + \mathcal{P})\overline{\Delta}. \tag{4}$$

The topological sliding surface for the platoon is defined by $S(t) = \mathbf{0}$.

Remark 1: Each sliding variable s_i depends on local node states, i.e., states of vehicle i as well as states of neighboring vehicles as constrained by the information topology. Note that $\Delta_i - \Delta_j$ does not depend on leader states since

$$\Delta_i - \Delta_j = v_i - v_j + \rho(x_i - x_j + d(i-j)).$$

Remark 2: The sliding variable S is a bijective linear function of $\bar{\Delta}$ defined in (4) because $\mathcal{L} + \mathcal{P}$ is invertible (see Lemma 1).

B. Design of topological reaching law

To design the DSMC controller, the reaching law has to conform with the associated sliding surface. The topological reaching law for node i is

$$\dot{s}_i = -\psi f_i^{ST}(S) - \phi f_i^{ST}(\mathrm{sgn}(S))$$

where ψ, $\phi \in \mathbb{R}^+$ are tuning parameters. Combining these for all nodes, we arrive at the compact form array

$$\dot{S} = -(\mathcal{L} + \mathcal{P})(\psi S + \phi\,\mathrm{sgn}(S)). \tag{5}$$

We observe that

$$(\mathcal{L} + \mathcal{P})\dot{\overline{\Delta}} = -(\mathcal{L} + \mathcal{P})(\psi S + \phi\,\mathrm{sgn}(S)).$$

Since $\mathcal{L} + \mathcal{P}$ is invertible, we obtain

$$\dot{\overline{\Delta}} = -(\psi S + \phi\,\mathrm{sgn}(S)). \tag{6}$$

Invertibility of $\mathcal{L} + \mathcal{P}$ is critical in designing a distributed SMC suitable for a broad range of topologies. Component i of the vector-valued equation (6) is then

$$\dot{\Delta}_i = -\psi s_i - \phi\,\mathrm{sgn}(s_i). \tag{7}$$

Differentiating (3) and equating the result to (7) provides an expression for $\dot{v}_i$. Substituting this in (2) yields the control law for node i:

$$\begin{aligned} T_i = &\frac{R_i}{\eta_i}(m_i f g + C_{A,i} v_i^2) - \frac{m_i R_i \rho}{\eta_i}(v_i - v_0) \\ &- \frac{m_i R_i}{\eta_i}(\psi s_i + \phi\,\mathrm{sgn}(s_i)). \end{aligned} \tag{8}$$

Remark 3: The control law (8) is not quite distributed because of its possible dependence on the leader velocity v_0. We therefore need to design a distributed observer for v_0 to derive a truly distributed control law. This is done in the next subsection.

C. Design of topologically structured velocity observer

Let $\hat{v}_{0,i}$ denote the estimation of v_0 produced by the i-th vehicle. The observer of i-th vehicle for the virtual leader's velocity is

$$\dot{\hat{v}}_{0,i} = -k s_i. \tag{9}$$

Since s_i is computed in a distributed fashion with (4), the observer is distributed (i.e., compatible with the underlying information topology). Using the estimated leader velocity $\hat{v}_{0,i}$ from the observer, the control law (8) becomes:

$$\begin{aligned} T_i = &\frac{R_i}{\eta_i}(m_i f g + C_{A,i} v_i^2) - \frac{m_i R_i \rho}{\eta_i}(v_i - \hat{v}_{0,i}) \\ &- \frac{m_i R_i}{\eta_i}(\psi s_i + \phi\,\mathrm{sgn}(s_i)). \end{aligned} \tag{10}$$

Remark 4: For simplicity, we have used second-order nonlinear node dynamics. Our approach easily generalizes to higher-order nonlinear dynamics. A regulation example with more complex vehicle dynamics is offered in our previous work [22].

IV. Main Stability Result

The stability analysis of DSMC is divided into two phases, i.e., the reaching phase and the sliding phase. The stability of the reaching phase is analyzed by Lyapunov method, while that of the sliding phase follows traditional SMC analysis.

A. Reaching Phase

We state our first main result:

Theorem 1: Consider a platoon with nonlinear node dynamics (1) and (2) with information topology under Assumption 1. Under the distributed control law (10) and tuning parameters ψ, ϕ, ρ, $k \in \mathbb{R}^+$, the sliding variable S in (4) and the observer error $\epsilon \triangleq [\hat{v}_{0,1} - v_0, \ldots, \hat{v}_{0,N} - v_0]^\top$ converge to $\mathbf{0}$ asymptotically.

Proof: With the sliding variable (4), velocity observer (9) and control law (10), the dynamics of (S, ϵ) becomes

$$\begin{aligned} \dot{S} &= (\mathcal{L} + \mathcal{P})(-\psi S - \phi\,\mathrm{sgn}(S) + \rho\epsilon), \\ \dot{\epsilon} &= -kS. \end{aligned} \tag{11}$$

The first equation of (11) is obtained by differentiating both sides of (4), and substituting (3), agent dynamics (1), (2), and control law (10) to the right-hand side of the equation.

For simpler presentation, define

$$\begin{aligned} \mathbf{x} &\triangleq \begin{bmatrix} S \\ \epsilon \end{bmatrix}, \\ f(\mathbf{x}) &\triangleq \begin{bmatrix} (\mathcal{L} + \mathcal{P})(-\psi S - \phi\,\mathrm{sgn}(S) + \rho\epsilon) \\ -kS \end{bmatrix}. \end{aligned} \tag{12}$$

To discuss the existence and stability of solution of a discontinuous system (11), we take the concepts of differential

inclusion and Filippov set-valued map from [23]. Since f is measurable and essentially locally bounded, then the associated Filippov set-valued map satisfies all the conditions of Lemma 2 (see appendix A), this guarantees the existence of Filippov solution.

The Filippov set-valued map associated with (12) is

$$\mathcal{F}[f](\mathbf{x}) = \left[\begin{array}{c} (\mathcal{L}+\mathcal{P})(\rho\epsilon - \psi S) \\ -kS \end{array} \right] - \left[\begin{array}{c} (\mathcal{L}+\mathcal{P})\phi\mathcal{W} \\ 0 \end{array} \right],$$

where $\mathcal{W}$ is the set defined by

$$\begin{aligned} \mathcal{W} = \text{co}\{\bar{S} = [\bar{s}_1, \cdots, \bar{s}_N]^\top \,|\, \bar{s}_i = \text{sgn}(s_i), \text{ if } s_i \neq 0; \\ \bar{s}_i = \{-1, 1\}, \text{ if } s_i = 0\}. \end{aligned} \tag{13}$$

We choose a Lyapunov candidate for the networked system,

$$V_1(\mathbf{x}) = \frac{1}{2}\mathbf{x}^\top \left[\begin{array}{cc} (\mathcal{L}+\mathcal{P})^{-1} & 0 \\ 0 & \frac{\rho}{k} I_N \end{array} \right] \mathbf{x}, \tag{14}$$

where I_N is the N dimensional identity matrix. The gradient of (14) is

$$\nabla V_1(\mathbf{x}) = \left[\begin{array}{c} (\mathcal{L}+\mathcal{P})^{-1} S \\ \frac{\rho}{k}\epsilon \end{array} \right].$$

Taking the Lie derivative of the Lyapunov candidate,

$$\begin{aligned} \tilde{\mathcal{L}}_{\mathcal{F}[f]} V_1(\mathbf{x}) =& \{\nabla V_1(\mathbf{x})^\top v \,|\, v \in \mathcal{F}[f](\mathbf{x})\} \\ =& \nabla V_1(\mathbf{x})^\top \mathcal{F}[f](\mathbf{x}) \\ =& -\psi S^\top S - \phi S^\top \mathcal{W}. \end{aligned} \tag{15}$$

The second term of (15) is

$$\begin{aligned} -\phi S^\top \mathcal{W} =& \{-\phi S^\top w \,|\, w \in \mathcal{W}\} \\ =& \{-\phi \sum_{i=1}^{N} s_i w_i \,|\, w \in \mathcal{W}\}, \end{aligned}$$

where w_i is the i-th element of w. Using the definition of $\mathcal{W}$ in (13), each $s_i w_i$ is

$$s_i w_i = \left\{ \begin{array}{ll} 0, & \text{if } s_i = 0, \\ s_i \,\text{sgn}(s_i), & \text{if } s_i \neq 0. \end{array} \right.$$

Hence,

$$-S^\top \phi \mathcal{W} = \{-\phi \sum_{i=1}^{N} s_i \,\text{sgn}(s_i)\} = \{-\phi \|S\|_1\}.$$

The Lie derivative $\tilde{\mathcal{L}}_{\mathcal{F}[f]} V_1(\mathbf{x})$ is therefore a singleton,

$$\tilde{\mathcal{L}}_{\mathcal{F}[f]} V_1(\mathbf{x}) = \{-\psi \|S\|_2^2 - \phi \|S\|_1\}. \tag{16}$$

We check the three conditions of Lemma 4 (see appendix A): i. $V_1(\mathbf{x})$ is continuously differentiable; ii. $V_1(\mathbf{x}) > 0$ for $\mathbf{x} \in \mathbb{R}^{2N} \setminus \{\mathbf{0}\}$; iii. By (16), $\max \tilde{\mathcal{L}}_{\mathcal{F}[f]} V_1(\mathbf{x}) \leq 0$. We conclude closed-loop system is stable in the sense of Lyapunov.

The next step is to prove asymptotic stability. For any initial condition $\mathbf{x}(0)$, choose a constant $c \geq V_1(\mathbf{x}(0))$, define Ω_c to be the level set of $V_1(\mathbf{x})$,

$$\Omega_c = \{\mathbf{x} = \left[\begin{array}{c} S \\ \epsilon \end{array} \right] \,|\, V_1(\mathbf{x}) \leq c\}. \tag{17}$$

From (16), Ω_c is positively invariant for all $c > 0$. Define

$$\begin{aligned} \mathcal{Z}_{F,V_1} \triangleq& \overline{\{\mathbf{x} \in \mathbb{R}^{2N} \,|\, 0 \in \tilde{\mathcal{L}}_{\mathcal{F}[f]} V_1(\mathbf{x})\}} \\ =& \{\mathbf{x} \,|\, S = \mathbf{0}\}. \end{aligned} \tag{18}$$

Then we have

$$\Omega_c \cap \mathcal{Z}_{F,V_1} = \{\mathbf{x} \,|\, S = \mathbf{0},\ \frac{\rho}{k}\|\epsilon\|_2^2 \leq 2c\}.$$

From (15), the largest weakly invariant set M in $\Omega_c \cap \mathcal{Z}_{F,V_1}$ is $M = \{\mathbf{x} \,|\, \mathbf{x} = \mathbf{0}\}$. Since the Lyapunov function $V_1(\mathbf{x})$ is radially unbounded, we can use Lemma 5 (see appendix A) to conclude global asymptotic stability. ■

Next, we offer a sufficient condition for finite-time convergence to the topological sliding surface $S = \mathbf{0}$.

Theorem 2: Consider again the assumptions and parameter settings of Theorem 1, with the set Ω_c and $\mathcal{Z}_{F,V_1}$ defined in (17) and (18). For all $c \in \{c_f | 0 < c_f < \frac{\phi^2}{2k\rho}\}$, the set $\mathcal{Z}_{F,V_1} \cap \Omega_c = \{(S,\epsilon) | S = \mathbf{0},\ \|\epsilon\|_2 \leq \sqrt{2ck/\rho}\}$ is positively invariant; and any solution $\mathbf{x}(t) = [S(t), \epsilon(t)]^\top$ of system (11) with initial condition $\mathbf{x}(0) \in \Omega_c$ reaches $\mathcal{Z}_{F,V_1} \cap \Omega_c$ in finite time.

Proof: To discuss the topological sliding surface dynamics, let us choose the Lyapunov candidate

$$V_2(S) = \frac{1}{2} S^\top (\mathcal{L}+\mathcal{P})^{-1} S. \tag{19}$$

The Lie derivative of (19) is

$$\begin{aligned} \tilde{\mathcal{L}}_{\mathcal{F}[f]} V_2(S) =& -\psi S^\top S - \phi S^\top \mathcal{W} + \rho \epsilon^\top S \\ =& \{-\psi \|S\|_2^2 - \phi \|S\|_1 + \rho \epsilon^\top S\}. \end{aligned} \tag{20}$$

Since we have already proved that the set Ω_c from (17) is positively invariant for any $c > 0$, if $\mathbf{x}(0) \in \Omega_c$, then

$$\|\epsilon(t)\|_2 \leq \sqrt{\frac{2ck}{\rho}}, \quad \forall t \in [0, +\infty).$$

With the condition $c < \frac{\phi^2}{2k\rho}$, we derive the upper bound of (20),

$$\begin{aligned} \max \tilde{\mathcal{L}}_{\mathcal{F}[f]} V_2(S) \leq& -\psi \|S\|_2^2 - (\phi - \sqrt{2ck\rho}) \|S\|_1 \\ <& 0. \end{aligned} \tag{21}$$

We can conclude that $\{\mathbf{x} \,|\, S = \mathbf{0}\} \cap \Omega_c$ is a positive-invariant set.

Next, we show finite-time convergence to S. Instead of proving the finite-time convergence of S directly, we prove that $\sqrt{2V_2} = \|(\mathcal{L}+\mathcal{P})^{-\frac{1}{2}} S\|_2$ converges to 0 in finite time.

In the region $\{\mathbf{x} | \mathbf{x} \in \Omega_c,\ s \neq \mathbf{0}\}$, the set-valued Lie derivative of $\sqrt{2V_2}$ is

$$\tilde{\mathcal{L}}_{\mathcal{F}[f]} \sqrt{2V_2} = \frac{1}{\|(\mathcal{L}+\mathcal{P})^{-\frac{1}{2}} S\|_2} \tilde{\mathcal{L}}_{\mathcal{F}[f]} V_2. \tag{22}$$

From (21), we have

$$\begin{aligned} &\max \tilde{\mathcal{L}}_{\mathcal{F}[f]} V_2(S) \\ &\quad \leq -\psi \|S\|_2^2 - (\phi - \sqrt{2ck\rho}) \|S\|_1 \\ &\quad \leq -\psi \|S\|_2^2 - \frac{1}{\sqrt{N}} (\phi - \sqrt{2ck\rho}) \|S\|_2. \end{aligned} \tag{23}$$

By Reyleigh's quotient, we have

$$\|(\mathcal{L}+\mathcal{P})^{-\frac{1}{2}}S\|_2 \leq \frac{1}{\sqrt{\lambda_{\min}(\mathcal{L}+\mathcal{P})}}\|S\|_2. \tag{24}$$

From (22), (23) and (24), one can establish

$$\max \tilde{\mathcal{L}}_{\mathcal{F}[f]}\sqrt{2V_2} \leq -\sqrt{\frac{\lambda_{\min}(\mathcal{L}+\mathcal{P})}{N}}(\phi-\sqrt{2ck\rho}),$$

for all $\{\mathbf{x}\,|\,\mathbf{x}\in\Omega_c,\, S\neq\mathbf{0}\}$.

From Lemma 3 (see Appendix A), we have

$$\frac{\mathrm{d}}{\mathrm{d}t}\|(\mathcal{L}+\mathcal{P})^{-\frac{1}{2}}S(t)\|_2 \in \tilde{\mathcal{L}}_{\mathcal{F}[f]}\sqrt{2V_2} \tag{25}$$

for almost every $t\in[0,+\infty)$. We have

$$\begin{aligned}\|(\mathcal{L}+\mathcal{P})^{-\frac{1}{2}}S(t_f)\|_2 =&\|(\mathcal{L}+\mathcal{P})^{-\frac{1}{2}}S(0)\|_2\\ &+\int_0^{t_f}\frac{\mathrm{d}}{\mathrm{d}\tau}\|(\mathcal{L}+\mathcal{P})^{-\frac{1}{2}}S(\tau)\|_2\mathrm{d}\tau.\end{aligned} \tag{26}$$

With (25) and (26), in the region $\{\mathbf{x}|\mathbf{x}\in\Omega_c,\, S\neq\mathbf{0}\}$ we have

$$\begin{aligned}\|(\mathcal{L}+\mathcal{P})^{-\frac{1}{2}}S(t_f)\|_2 \leq& \|(\mathcal{L}+\mathcal{P})^{-\frac{1}{2}}S(0)\|_2\\ &-t_f(\phi-\sqrt{2ck\rho})\sqrt{\frac{\lambda_{\min}(\mathcal{L}+\mathcal{P})}{N}}.\end{aligned} \tag{27}$$

We argue that there must exist t_f such that $S(t_f)=\mathbf{0}$. Otherwise, $\|(\mathcal{L}+\mathcal{P})^{-\frac{1}{2}}S(t_f)\|_2\to-\infty$ as $t_f\to+\infty$. ■

Remark 5: The above result establishes that every trajectory starting in Ω_c approaches $\{(S,\epsilon)|S=\mathbf{0},\, \|\epsilon\|_2\leq\sqrt{2ck/\rho}\}$ in finite time. By choosing c sufficiently large, any compact set in $\mathbb{R}^{2N}$ will fall inside Ω_c. As a result, $\frac{\phi^2}{2k\rho}$ can be made arbitrary large, and Theorem 2 offers a sufficient semi-global condition for finite-time convergence to the sliding surface.

B. Sliding Phase

Theorem 3: Consider a vehicle platoon with nonlinear dynamics described by (1) and (2) and information topology under Assumption 1. During the sliding phase where $S=\mathbf{0}$, the tracking error for each vehicle $e_i\to 0$ as $t\to\infty$.

Proof: In the sliding surface $S=\mathbf{0}$, with the definition of sliding error, we have

$$S=(\mathcal{L}+\mathcal{P})\overline{\Delta}=\mathbf{0}.$$

With $\mathcal{L}+\mathcal{P}$ being positive definite, we have

$$\overline{\Delta}=[\Delta_1,\,\Delta_2,\ldots,\Delta_N]^\top=\mathbf{0}.$$

For each Δ_i,

$$\Delta_i=\dot{e}_i+\rho e_i=0, \tag{28}$$

where $\rho>0$. Hence (28) is a stable differential equation, $e_i\to 0$ as $t\to\infty$. ■

Due to practical realities of switching devices, the control law (10) can cause chattering. The following result assures that asymptotic stability of (11) is preserved with a smooth control law by setting $\phi=0$.

Corollary 1: Consider again the set-up and assumptions of Theorem 1 with tuning parameter $\psi,k\in\mathbb{R}^+$ and $\phi=0$. Then, the closed-loop system (11) is asymptotic stable.

Proof: By setting $\phi=0$, the closed-loop system (11) becomes linear

$$\dot{\mathbf{x}}(t)=A\mathbf{x}(t), \tag{29}$$

where A is defined as

$$A\triangleq\begin{bmatrix}-\psi(\mathcal{L}+\mathcal{P}) & \rho(\mathcal{L}+\mathcal{P})\\ -kI_N & 0\end{bmatrix}. \tag{30}$$

Let

$$P\triangleq\begin{bmatrix}\frac{k}{\psi}(\mathcal{L}+\mathcal{P})^{-1}+\frac{\rho}{\psi}I_N & -I_N\\ -I_N & \frac{\rho}{\psi}I_N+(\frac{\rho^2}{\psi k}+\frac{\psi}{k})(\mathcal{L}+\mathcal{P})\end{bmatrix}.$$

Using the characterization of positive definite matrices with Schur complements [24] to prove matrix P is positive definite, two conditions have to be satisfied:

i. The first diagonal block is positive definite

$$\frac{k}{\psi}(\mathcal{L}+\mathcal{P})^{-1}+\frac{\rho}{\psi}I_N\succ 0.$$

ii. The Schur complements is positive definite

$$\begin{aligned}&\frac{\rho}{\psi}I_N+(\frac{\rho^2}{\psi k}+\frac{\psi}{k})(\mathcal{L}+\mathcal{P})\\ &\quad-(\frac{k}{\psi}(\mathcal{L}+\mathcal{P})^{-1}+\frac{\rho}{\psi}I_N)^{-1}\succ 0.\end{aligned}$$

One can check easily that the first condition holds since $\mathcal{L}+\mathcal{P}$ is positive definite. The second part is proved by using the matrix inversion lemma (Woodbury matrix identity) [25]. Since the algebraic process is simple, we omit this part for brevity.

Next, choose a Lyapunov candidate $V_3(\mathbf{x})=\frac{1}{2}\mathbf{x}^\top P\mathbf{x}$. The derivative of $V_3(\mathbf{x})$ with respect to system (29) is

$$\begin{aligned}\dot{V}_3(\mathbf{x}) =&\frac{1}{2}\mathbf{x}^\top(A^\top P+PA)\mathbf{x}\\ =&-\mathbf{x}^\top Q\mathbf{x}<0,\end{aligned} \tag{31}$$

where matrix Q is defined as the positive definite matrix

$$Q\triangleq\rho\begin{bmatrix}(\mathcal{L}+\mathcal{P}) & 0\\ 0 & (\mathcal{L}+\mathcal{P})\end{bmatrix}\succ 0.$$

We conclude matrix A is Hurwitz. ■

Remark 6: By eliminating the switching term, the asymptotic stability result of Theorem 1 is preserved, however, the finite-time convergence property from Theorem 2 is compromised. As is done with traditional SMC, a suitable trade-off between tracking precision and finite-time convergence can be arranged by introducing a thin boundary layer neighboring the topological sliding surface, $\{S\,|\,\|S\|_2\leq\varepsilon\}$. Using the negative definiteness condition (31), one can prove that the boundary layer is invariant and can be reached in finite time. Within the boundary layer, the tracking error for each vehicle remains bounded.

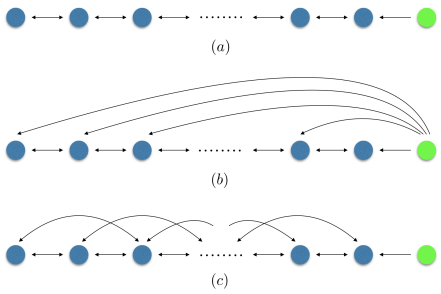

Fig. 3. Types of bidirectional information flow topology used in this paper: (a) nearest-neighbor (NN); (b) nearest-neighbor with leader paths (NNL); (c) two-nearest-neighbor (2NN).

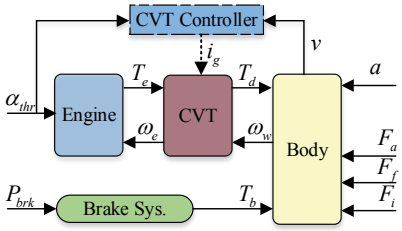

Fig. 4. Sketch of vehicle longitudinal dynamics.

V. Robust Performance of DSMC

In this section, we analyze the performance of DSMC under external disturbance. For theoretical simplicity, we assume tuning parameter $\phi = 0$.

Assume all vehicles are subject to persistent external disturbances δ_i:

$$\begin{aligned}\dot{x}_i(t) =& v_i(t),\\ \dot{v}_i(t) =& \frac{1}{m_i}\left(\eta_i \frac{T_i(t)}{R_i} - C_{A,i} v_i^2(t)\right) - gf + \delta_i(t),\end{aligned}$$

and the acceleration of the virtual leader is non-zero $\dot{v}_0 = \delta_0(t)$. The acceleration of the virtual leader is unknown.

The closed-loop dynamics (11) with external disturbances becomes

$$\dot{\mathbf{x}}(t) = A\mathbf{x}(t) + Bd(t), \tag{32}$$

where $\mathbf{x} = [S, \epsilon]^\top$, A is defined in (30), B and $d(t)$ is defined as

$$B \triangleq \begin{bmatrix} \mathcal{L}+\mathcal{P} \\ 0 \end{bmatrix} \text{ and } d \triangleq \begin{bmatrix} \delta_1 - \delta_0 \\ \vdots \\ \delta_N - \delta_0 \end{bmatrix}.$$

The Hurwitz A matrix implies the Input-to-State Stability (ISS) of system (32):

$$\begin{aligned}\mathbf{x}(t) =& e^{At}\mathbf{x}(0) + \int_0^t e^{A(t-\tau)} Bd(\tau)\mathrm{d}\tau,\\ |\mathbf{x}(t)| \leq& \|e^{At}\||\mathbf{x}(0)| + \int_0^t \|e^{A(t-\tau)}\|\|B\||d(\tau)|\mathrm{d}\tau\\ \leq& \kappa e^{-\alpha t}|\mathbf{x}(0)| + \|B\| \sup_{\tau\in[0,t]}|d(\tau)| \int_0^t \kappa e^{-\alpha t}\mathrm{d}\tau\\ \leq& \kappa e^{-\alpha t}|\mathbf{x}(0)| + \frac{\kappa}{\alpha}\|B\| \sup_{\tau\in[0,t]}|d(\tau)|,\end{aligned} \tag{33}$$

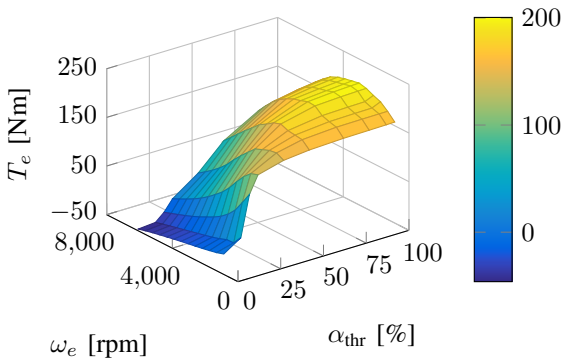

Fig. 5. Engine torque map.

where $|\cdot|$ denotes vector norm (e.g 1, 2, ∞ norm) in Euclidean space, $\|\cdot\|$ denotes the corresponding matrix norm, $\kappa, \alpha \in \mathbb{R}_+$ and $\max \mathrm{Re}\{\lambda(A)\} < -\alpha$. We further define:

$$\begin{aligned}\beta(|\mathbf{x}(0)|, t) \triangleq& \kappa e^{-\alpha t}|\mathbf{x}(0)|,\\ \gamma(\sup_{\tau\in[0,t]}|d(\tau)|) \triangleq& \frac{\kappa}{\alpha}\|B\| \sup_{\tau\in[0,t]}|d(\tau)|.\end{aligned}$$

We can easily check function β is class-$\mathcal{KL}$ and γ is class-$\mathcal{K}$, then conclude ISS.

Remark 7: The disturbance attenuation effect is closely related to $\max \mathrm{Re}\{\lambda(A)\}$. For a smaller $\max \mathrm{Re}\{\lambda(A)\}$, the error bound of $\mathbf{x}(t)$ will be smaller. From (30), we observe that the eigenvalues of A are affected by the information flow topology $\mathcal{L}+\mathcal{P}$ and the tuning parameters ψ, ρ.

Remark 8: The inequality (33) is related to *collision avoidance*. The sliding variable S is bounded due to the boundness of $\mathbf{x}(t)$. Sliding variable S and $\overline{\Delta}$ are isomorphic (4). Each Δ_i and tracking error e_i are related through a stable linear system (3):

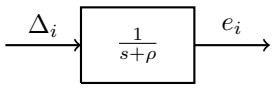

We can conclude tracking error e_i is bounded. Then we can guarantee collision avoidance for finite length platoon if properly selecting spacing policy, tuning parameter and information flow topology [26].

Remark 9: Since system (32) is ISS, if $\delta_i(t) = 0$ for all $i \in \mathcal{N}$, and δ_0 eventually converges to 0, then the tracking error $e_i \to 0$ as $t \to 0$.

VI. Simulation Results

We now illustrate the effectiveness of proposed DSMC through numerical simulations. A heterogeneous platoon with 1 leader and 8 followers is simulated under 3 different information flow topologies. These topologies are nearest-neighbor (NN), nearest-neighbor with leader paths (NNL), and two-nearest-neighbor (2NN), as shown in Fig. 3. With the NNL topology, all the vehicles have access to the leader. This will allow us to demonstrate effect of the leader information on the performance of the platoon.

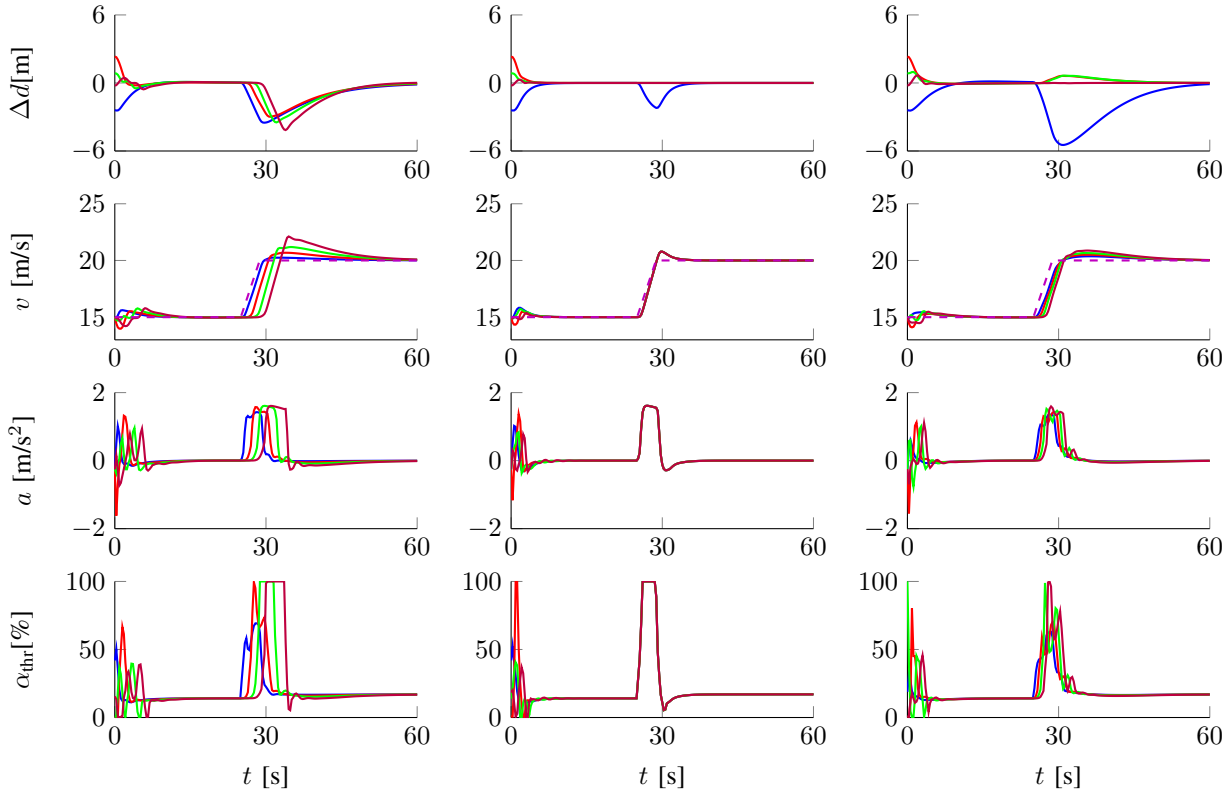

(a) NN (b) NNL (c) 2NN

Fig. 6. Simulation result in ramp speed profile under NN, NNL, and 2NN topologies. 1st, 3rd, 5th, and 7th vehicle are denoted by (——), (——), (——), and (——), respectively. (- - -) denotes leader velocity.

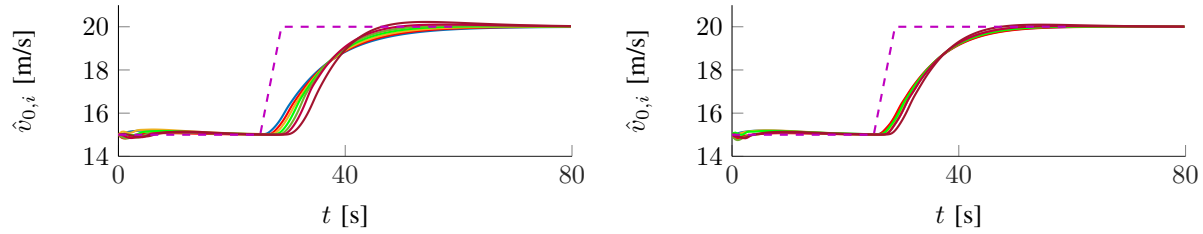

(a) NN (b) 2NN

Fig. 7. Result of topologically structured velocity observer. The map between vehicles and lines are: 2nd vehicle (——), 3rd vehicle (——), 4th vehicle (——), 5th vehicle (——), 6th vehicle (——), 7th vehicle (——), 8th vehicle (——).

The distributed control law (10) was designed based on a nonlinear vehicle dynamics (1)-(2) for simplicity and elegance. In the simulation, we applied the control law to platoon with high-fidelity vehicle model to validate the performance of DSMC under modeling uncertainty. Each vehicle is a passenger car with a gasoline engine, a torque converter, a continuous variable transmission (CVT), two driving and two driven wheels, as well as a hydraulic braking system. Fig. 4 sketches the powertrain dynamics. The inputs are the throttle angle (α_{thr}) and the braking pressure (P_{brk}). In realistic driving modes, a driver can not simultaneously engage the throttle and brake pedals. Therefore, in this study we use an inverse model to allocate the driving commands (T_i) to either throttle angle or braking pressure. Interested readers can refer to [27] for further information. The outputs include the longitudinal acceleration (a), vehicle velocity (v), as well as other measurable variables in the powertrain. When driving, the engine torque is amplified by the torque converter, CVT, and final gearing and acts on the two front driving wheels. When braking, the braking torque acts on all four wheels to dissipate the kinetic energy of the vehicle body. Fig. 5 shows the nonlinear engine torque map: engine torque (T_e) is a nonlinear monotonically increasing function of engine speed (ω_e) and throttle angle (α_{thr}). The vehicle parameters are offered in Table I, in which the heterogeneity is represented by the difference in vehicle mass (m_i) and wheel radius (R_i). In addition, parameter uncertainties are added in mechanical efficiency (η_i), coefficient of aerodynamic drag ($C_{A,i}$), and coefficient of rolling resistance (f). In this study, the parameter heterogeneities are known while the parameter uncertainties are unknown.

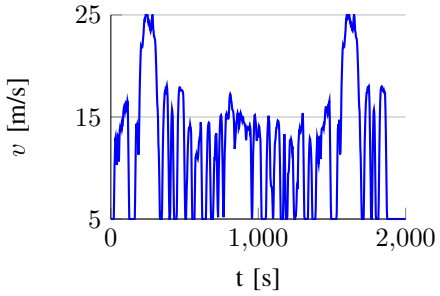

Fig. 8. The velocity profile of leading vehicle when running EPA74 standard driving cycle.

Parameter	Value	Uncertainty
m_i	$(1445 + i \times 50)$ kg	0%
η_i	0.85	$\pm$10%
$C_{A,i}$	0.43 kg/ m	$\pm$10%
R_i	$(0.28 + i \times 0.005)$m	0%
f	0.02	$\pm$10%

TABLE I
SIMULATION PARAMETERS

The simulation includes 2 scenarios distinguished by the speed profile of leading vehicle: constant speed ramp and modified EPA74 profile. In the former, the leading vehicle ramps from 15m/s to 20m/s in 3 seconds with constant acceleration, for the purpose of examine the stability of the distributed control law. In the latter, the leading vehicle follows a modified EPA74 speed profile to allow comparison of platooning performance under different communication topologies.

A. Simulation of Leader's Ramp Speed Profile

The simulation results of the 3 topologies, i.e., NN, NNL, and 2NN, are shown in Fig. 6 (a)-(c) respectively. In each figure, there are 4 subplots from top to bottom, including distance error between 2 consecutive vehicles ($\Delta d_i = e_i - e_{i-1}$), vehicle velocity ($v_i$), vehicle acceleration (a_i), and throttle angle ($\alpha_{\text{thr},i}$). One can observe that the tracking error converges to zero asymptotically for both non-zero initial condition and time-varying leader velocity. The velocity estimation of NN and 2NN topology is shown in Fig. 7.

B. Simulation of modified EPA74 speed profile

The simulation results are shown in Fig. 9. The used speed profile, shown in Fig 8, is modified from the standard EPA74 by multiplying 0.8 and then adding 5m/s point-wise. Three performance indices – tracking index (TI), acceleration standard deviation (ASD), and fuel economy (Fuel) – are used to assess the performance. The tracking index for i-th vehicle is calculated by

$$\text{TI}_i = \frac{1}{T}\int_0^T \left(|\dot{e}_i(t) \cdot SVE| + |\Delta d_i(t) \cdot SDE|\right) \mathrm{d}t,$$

where T is the simulation length, $SVE = 10$ denotes sensitivity of velocity error, and $SDE = 1$ denotes sensitivity to distance error [28]. The ASD for i-th vehicle is calculated by

$$\text{ASD}_i = \text{std}(a_i(t)),$$

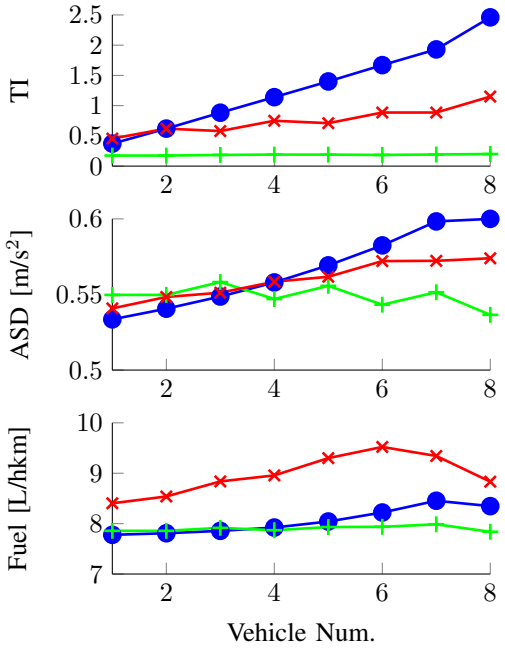

Fig. 9. Simulation result under EPA74 scenario. From top to bottom, each subplot shows tracking index, acceleration standard deviation and fuel consumption for each vehicle. The NN, NNL, and 2NN are denoted by (—●—), (—+—), and (—×—).

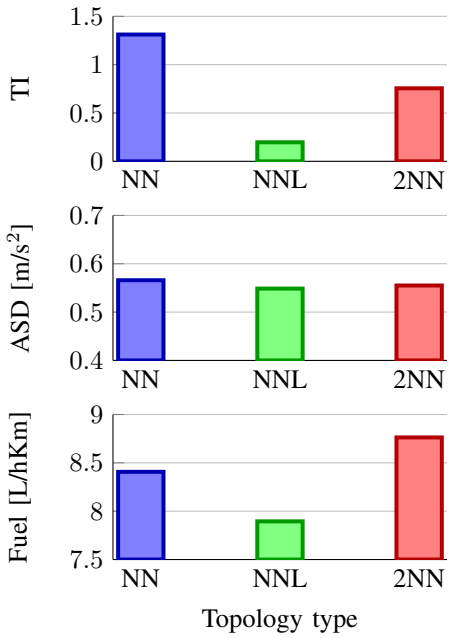

Fig. 10. Performance analysis of 3 different topologies. Each subplot shows average performance indexes.

where std denotes standard deviation in $t \in [0, T]$. The fuel economy for i-th vehicle is calculated with

$$\text{Fuel}_i = \frac{\int_0^T Q_i(t)\mathrm{d}t}{x_i(T)},$$

where Q_i denotes the engine fuel injecting rate and $x_i(t)$ is the traveling distance.

We observe from Fig. 9 that 2NN has superior tracking performance compared to NN, due to access to more information from neighboring nodes, in combination with the constant-distance spacing policy. The topology with full leader access (NNL), have significantly improved tracking ability compared with other topologies. These results confirm our intuitive analysis. The topological selection has less influence on the acceleration noise. In addition it is found that 2NN has the worse fuel economy than NN. This phenomenon is caused by more aggressive control inputs, which come from a tighter information connection with other neighboring vehicles. More neighbor information is then beneficial to the tracking capability but unfavorable to the fuel economy. Fortunately, more leading information contributes to both tracking capability and fuel economy. Similar conclusions can be drawn from Fig. 10.

Remark 10: We used a high-fidelity model in this section. The simulation result (tracking performance, velocity profile and acceleration) of the design model (1)-(2) is similar to the result presented in this section.

VII. Conclusion

We have proposed a distributed SMC for nonlinear heterogeneous vehicular platoons with positive definite topologies. The DSMC is able to deal with information topology diversity by introducing a novel topologically structured function to design the sliding surface and reaching law. Our design relies on the assumption that the information flow topology among the followers is bi-directional connected and that the leader is connected to at least one follower to arrive at a sliding mode controller that is distributed. The stability of the discontinuous closed-loop system is proved in the sense of Filippov and verified via numerical simulation.

The performance of our DSMC method can be enhanced by incorporating other nonlinear control methods into our basic framework. For example, the intermediate error Δ_i, which is designed with a linear stable differential function, can be formulated with backstepping control for higher-order systems, multiple surface sliding control (MSSC) for dynamics with mismatched uncertainty and dynamic surface control (DSC) to mitigate the "explosion of terms" phenomenon. From a broader view, we see the potential of this DSMC framework for general multi-agent consensus problem and synchronization of complex networks that can deal with dynamical nonlinearity, heterogeneity, and topology variety.

Acknowledgments

This study is partially supported by NSF Award CNS-1446891, NSF China with 51575293 and 51622504, National Key R&D Program of China with 2016YFB0100906, and International Sci&Tech Cooperation Program of China under 2016YFE0102200.

The author wishes to thank Murat Arcak, Andrew Packard and anonymous reviewers for their valuable suggestions.

Appendix A
Discontinuous Systems

Sliding mode control is used to stabilize a platoon by intentionally introducing discontinuities in the feedback loop [29]. The closed-loop dynamics with discontinuity do not satisfy the traditional Lipschitz conditions that assure the existence and the uniqueness of continuous differentiable solutions. Solutions of discontinuous ordinary differential equations can be analyzed using Filippov methods [30]. Our exposition here follows [23].

Consider the vector-valued ordinary differential equation

$$\dot{x}(t) = f(x(t)). \tag{34}$$

Here, $x(t) \in \mathbb{R}^n$, $f : \mathbb{R}^n \to \mathbb{R}^n$, and f is discontinuous. Let $\mathfrak{B}(\mathbb{R}^n)$ be the collection of all subsets of $\mathbb{R}^n$. The Filippov set-valued map $\mathcal{F}[f] : \mathbb{R}^n \to \mathfrak{B}(\mathbb{R}^n)$ associated with f is defined as

$$\mathcal{F}[f](x) \triangleq \bigcap_{\delta>0} \bigcap_{\mu(H)=0} \overline{\text{co}}\{f(B(x, \delta) \setminus H)\}, \ x \in \mathbb{R}^n,$$

where $B(x, \delta)$ is a open ball of radius $\delta > 0$ centered at x, and the intersection is taken over all sets H with zero Lebesgue measure.

An absolutely continuous function $x(t) : [0, T] \to \mathbb{R}^n$ is said to be a solution of (34) in the sense of Filippov if for almost all $t \in [0, T]$,

$$\dot{x}(t) \in \mathcal{F}[f](x(t)). \tag{35}$$

The point x_e is an equilibrium of the differential inclusion (35) if $0 \in \mathcal{F}[f](x_e)$.

Lemma 2: [23] (*Existence of Filippov solution*) Let $f : \mathbb{R}^n \to \mathbb{R}^n$ be measurable and locally essentially bounded, i.e., bounded on a bounded neighborhood of every point, excluding sets of measure zero. Then for all $x_0 \in \mathbb{R}^n$, there exists a Filippov solution of (34) with initial condition $x(0) = x_0$.

Filippov solutions for discontinuous system are not necessary unique for each initial condition. Therefore, when considering properties such as stability in the sense of Lyapunov, asymptotic stability and invariance, we must specify whether attention is being paid to a particular solution starting from an initial condition ("weak") or to all the solutions starting from an initial condition ("strong"). For example, "weakly stable equilibrium point" means that at least one solution starting close to the equilibrium point remains close to it, whereas "strongly stable equilibrium point" means that all solutions starting close to the equilibrium point remain close to it. Detailed definitions can be found in [30], [23].

The Lie derivative of a set-valued map is defined as follows. Given a locally Lipschitz function $V : \mathbb{R}^n \to \mathbb{R}$ and a set-valued map $\mathcal{F} : \mathbb{R}^n \to \mathfrak{B}(\mathbb{R}^n)$, the set-valued Lie derivative $\tilde{\mathcal{L}}_{\mathcal{F}} V : \mathbb{R}^n \to \mathfrak{B}(\mathbb{R}^n)$ of V with respect to $\mathcal{F}$ at x is defined as

$$\tilde{\mathcal{L}}_{\mathcal{F}} V(x) \triangleq \{a \in \mathbb{R} : \text{ there exists } v \in \mathcal{F}(x), \text{ such that } \xi^\top v = a \text{ for all } \xi \in \partial V(x)\},$$

where $\partial V(x)$ denotes the generalized gradient [31]. If the function $V(x)$ is continuously differentiable, the generalized Lie derivative takes the following form:

$$\tilde{\mathcal{L}}_{\mathcal{F}} V(x) \triangleq \left\{\nabla V(x)^\top v : v \in \mathcal{F}(x)\right\}.$$

Lemma 3: Let $x : [0, t_1] \to \mathbb{R}^n$ be a solution of the differentiable inclusion (35), and let $V : \mathbb{R}^n \to \mathbb{R}$ be locally Lipschitz and regular. Then,

i. The composition $t \mapsto V(x(t))$ is differentiable at almost all $t \in [0, t_1]$.
ii. The derivative of $t \mapsto V(x(t))$ satisfies

$$\frac{\mathrm{d}}{\mathrm{d}t}(V(x(t))) \in \tilde{\mathcal{L}}_{\mathcal{F}} V(x(t)) \quad \text{for a.e. } t \in [0,\, t_1].$$

Lemma 4: [23] (*Discontinuous Lyapunov theorem*) Let $f : \mathbb{R}^n \to \mathbb{R}^n$ satisfy the hypotheses of Lemma 2, and $\mathcal{F}[f] : \mathbb{R}^n \to \mathfrak{B}(\mathbb{R}^n)$ be the set-valued map corresponding to f. Let x_e be an equilibrium of the differential inclusion (35), and let $\mathcal{D} \subset \mathbb{R}^n$ be an open and connected set with $x_e \in \mathcal{D}$. Furthermore, let $V : \mathbb{R}^n \to \mathbb{R}$ be such that the following holds:

i. V is locally Lipschitz and regular on $\mathcal{D}$.
ii. $V(x_e) = 0$, and $V(x) > 0$ for $x \in \mathcal{D} \setminus \{x_e\}$.
iii. $\max \tilde{\mathcal{L}}_{\mathcal{F}} V(x) \leq 0$ for each $x \in \mathcal{D}$.

Then x_e is a strongly stable equilibrium of (35). Note that a continuously differentiable function is automatically locally Lipschitz and regular, and hence one can invoke Lemma 4 for such functions.

Lemma 5: [23] (*Discontinuous Lasalle's invariance principle*) Let $f : \mathbb{R}^n \to \mathbb{R}^n$ satisfy the hypotheses of Lemma 2, and let $\mathcal{F}[f] : \mathbb{R}^n \to \mathfrak{B}(\mathbb{R}^n)$ be the set-valued map corresponding to f. Let $\Omega \subset \mathbb{R}^n$ be compact and strongly invariant for (35), and assume $\max \tilde{\mathcal{L}}_{\mathcal{F}} V(x) \leq 0$ for each $x \in \Omega$. Then, all solutions $x : [0, \infty) \to \mathbb{R}^n$ of (35) starting at Ω converge to the largest weakly invariant set M contained in

$$\Omega \cap \mathcal{Z}_{\mathcal{F},V},$$

where $\mathcal{Z}_{\mathcal{F},V} = \overline{\{x \in \mathbb{R}^n : 0 \in \tilde{\mathcal{L}}_{\mathcal{F}} V(x)\}}$.

APPENDIX B
PROOFS OF LEMMAS

A. Proof of Lemma 1

Proof: When G is undirected and connected, $\mathcal{L}$ is positive semi-definite, and the algebraic multiplicity of the zero eigenvalue is one. The eigenvector corresponding to zero eigenvalue is $\mathbf{1} \triangleq [1, 1, \ldots, 1]^\top \in \mathbb{R}^N$ [32]. Define eigenvalues of $\mathcal{L}$ to be $\lambda_1 = 0 < \lambda_2 \leq \ldots \leq \lambda_N$, and the corresponding eigenvectors are $\eta_1, \eta_2, \ldots, \eta_N$, where $\eta_1 = \mathbf{1}$. Since $\mathcal{L}$ is symmetric, it can be diagonalized by a orthogonal matrix composed of N linearly independent eigenvectors, so any vector $x \in \mathbb{R}^N$ can be written as a linear combination of the eigenvectors, $x = \sum_{i=1}^{N} c_i \eta_i$, where $c_i,\ i \in \mathcal{N}$ are constants. Since G contains a spanning tree, $\mathcal{P} \neq 0$, and $\eta_1^\top \mathcal{P} \eta_1 > 0$. For any $x \neq 0$, there is

$$x^\top (\mathcal{L} + \mathcal{P}) x = \sum_{i=2}^{N} \lambda_i c_i^2 \eta_i^\top \eta_i + x^\top \mathcal{P} x > 0.$$

■

REFERENCES

[1] R. Horowitz and P. Varaiya, "Control design of an automated highway system," *Proceedings of the IEEE*, vol. 88, no. 7, pp. 913–925, July 2000.

[2] Y. Zheng, S. Eben Li, J. Wang, D. Cao, and K. Li, "Stability and scalability of homogeneous vehicular platoon: Study on the influence of information flow topologies," *Intelligent Transportation Systems, IEEE Transactions on*, vol. 17, no. 1, pp. 14–26, 2016.

[3] S. Shladover, C. Desoer, J. Hedrick, M. Tomizuka, J. Walrand, W.-B. Zhang, D. McMahon, H. Peng, S. Sheikholeslam, and N. McKeown, "Automated vehicle control developments in the path program," *Vehicular Technology, IEEE Transactions on*, vol. 40, no. 1, pp. 114–130, Feb 1991.

[4] D. Swaroop, J. Hedrick, C. Chien, and P. Ioannou, "A comparision of spacing and headway control laws for automatically controlled vehicles," *Vehicle System Dynamics*, vol. 23, no. 1, pp. 597–625, 1994.

[5] D. Swaroop and J. Hedrick, "String stability of interconnected systems," *Automatic Control, IEEE Transactions on*, vol. 41, no. 3, pp. 349–357, Mar 1996.

[6] Y. Zheng, S. E. Li, K. Li, and L.-Y. Wang, "Stability margin improvement of vehicular platoon considering undirected topology and asymmetric control," *Control Systems Technology, IEEE Transactions on*, vol. pp, no. 99, 2016.

[7] L. Xiao and F. Gao, "Practical string stability of platoon of adaptive cruise control vehicles," *Intelligent Transportation Systems, IEEE Transactions on*, vol. 12, no. 4, pp. 1184–1194, Dec 2011.

[8] E. Shaw and J. Hedrick, "String stability analysis for heterogeneous vehicle strings," *American Control Conference*, pp. 3118–3125, July 2007.

[9] S. E. Li, Y. Zheng, K. Li, and J. Wang, "An overview of vehicular platoon control under the four-component framework," in *Intelligent Vehicles Symposium (IV), 2015 IEEE*. IEEE, 2015, pp. 286–291.

[10] J. Hedrick, D. McMahon, V. Narendran, and D. Swaroop, "Longitudinal vehicle controller design for ivhs systems," in *American Control Conference, 1991*. IEEE, 1991, pp. 3107–3112.

[11] A. Ferrara and C. Vecchio, "Second order sliding mode control of vehicles with distributed collision avoidance capabilities," *Mechatronics*, vol. 19, no. 4, pp. 471–477, 2009.

[12] T. Willke, P. Tientrakool, and N. Maxemchuk, "A survey of inter-vehicle communication protocols and their applications," *Communications Surveys Tutorials, IEEE*, vol. 11, no. 2, pp. 3–20, Second 2009.

[13] J.-W. Kwon and D. Chwa, "Adaptive bidirectional platoon control using a coupled sliding mode control method," *IEEE Transactions on Intelligent Transportation Systems*, vol. 15, no. 5, pp. 2040–2048, 2014.

[14] P. Barooah, P. Mehta, and J. Hespanha, "Mistuning-based control design to improve closed-loop stability margin of vehicular platoons," *Automatic Control, IEEE Transactions on*, vol. 54, no. 9, pp. 2100–2113, Sept 2009.

[15] J. Ploeg, D. P. Shukla, N. van de Wouw, and H. Nijmeijer, "Controller synthesis for string stability of vehicle platoons," *IEEE Transactions on Intelligent Transportation Systems*, vol. 15, no. 2, pp. 854–865, April 2014.

[16] R. Olfati-Saber and R. Murray, "Consensus problems in networks of agents with switching topology and time-delays," *Automatic Control, IEEE Transactions on*, vol. 49, no. 9, pp. 1520–1533, Sept 2004.

[17] X. Liu, A. Goldsmith, S. S. Mahal, and J. K. Hedrick, "Effects of communication delay on string stability in vehicle platoons," in *ITSC 2001. 2001 IEEE Intelligent Transportation Systems. Proceedings (Cat. No.01TH8585)*, 2001, pp. 625–630.

[18] G. Lee and S. Kim, "A longitudinal control system for a platoon of vehicles using a fuzzy-sliding mode algorithm," *Mechatronics*, vol. 12, no. 1, pp. 97–118, 2002.

[19] X. Guo, J. Wang, F. Liao, and R. S. H. Teo, "Distributed adaptive integrated-sliding-mode controller synthesis for string stability of vehicle platoons," *IEEE Transactions on Intelligent Transportation Systems*, vol. 17, no. 9, pp. 2419–2429, 2016.

[20] D. Swaroop and J. Hedrick, "Direct adaptive longitudinal control of vehicle platoons," in *Conference of Decision and Control, 1994*. IEEE, 1994, pp. 5116–5121.

[21] S. Eben Li, H. Peng, K. Li, and J. Wang, "Minimum fuel control strategy in automated car-following scenarios," *Vehicular Technology, IEEE Transactions on*, vol. 61, no. 3, pp. 998–1007, 2012.

[22] Y. Wu, S. E. Li, Y. Zheng, and J. K. Hedrick, "Distributed sliding mode control for multi-vehicle systems with positive definite topologies," in *2016 IEEE 55th Conference on Decision and Control (CDC)*, Dec 2016, pp. 5213–5219.

[23] J. Cortes, "Discontinuous dynamical systems," *IEEE Control Systems Magazine*, vol. 28, no. 3, pp. 36–73, 2008.

[24] F. Zhang, *The Schur complement and its applications*. Springer Science & Business Media, 2006, vol. 4.

[25] M. A. Woodbury, "Inverting modified matrices," *Memorandum report*, vol. 42, no. 106, p. 336, 1950.
[26] S. K. Yadlapalli, S. Darbha, and K. Rajagopal, "Information flow and its relation to stability of the motion of vehicles in a rigid formation," *IEEE Transactions on Automatic Control*, vol. 51, no. 8, pp. 1315–1319, 2006.
[27] S. E. Li, F. Gao, D. Cao, and K. Li, "Multiple-model switching control of vehicle longitudinal dynamics for platoon-level automation," *IEEE Transactions on Vehicular Technology*, vol. 65, no. 6, pp. 4480–4492, 2016.
[28] S. Eben Li, K. Li, and J. Wang, "Economy-oriented vehicle adaptive cruise control with coordinating multiple objectives function," *Vehicle System Dynamics*, vol. 51, no. 1, pp. 1–17, 2013.
[29] V. I. Utkin, *Sliding modes in control and optimization*. Springer Science & Business Media, 2013.
[30] A. F. Filippov, *Differential equations with discontinuous righthand sides: control systems*. Springer Science & Business Media, 2013, vol. 18.
[31] F. H. Clarke, *Optimization and nonsmooth analysis*. SIAM, 1990.
[32] C. Godsil and G. F. Royle, *Algebraic graph theory*. Springer Science & Business Media, 2013, vol. 207.

Yujia Wu received the B.S. degree in Automation Science and Electrical Engineering from Beihang University, Beijing, China, in 2013. He is now perusing the Ph.D. degree in Mechanical Engineering from University of California at Berkeley, USA. He is a member of Vehicle Dynamics & Control Lab. His research interests are in the area of nonlinear dynamical systems analysis and control design, complex networked systems, and distributed motion coordinate for groups of autonomous agents.

Shengbo Eben Li received the M.S. and Ph.D. degrees from Tsinghua University in 2006 and 2009. He worked at Stanford University, University of Michigan, and University of California Berkeley. He is currently a tenured associate professor in Department of Automotive Engineering at Tsinghua University. His research interests include intelligent vehicles and driver assistance, reinforcement learning and distributed control, optimal control and estimation, etc. He is the author of over 100 peer-reviewed journal/conference papers, and the co-inventor of over 20 Chinese patents. Dr. Li was the recipient of Best Paper Award in 2014 IEEE ITS Symposium, Best Paper Award in 14th ITS Asia Pacific Forum, National Award for Technological Invention in China (2013), Excellent Young Scholar of NSF China (2016), Young Professorship of Changjiang Scholar Program (2016). He is now the IEEE senior member, and serves as the TPC member of IEEE IV Symposium, ISC member of FAST-zero 2017 in Japan, Associated editor of IEEE ITSM and IEEE Trans ITS, etc.

Jorge Cortés received the Licenciatura degree in mathematics from Universidad de Zaragoza, Zaragoza, Spain, in 1997, and the Ph.D. degree in engineering mathematics from Universidad Carlos III de Madrid, Madrid, Spain, in 2001. He held postdoctoral positions with the University of Twente, Twente, The Netherlands, and the University of Illinois at Urbana-Champaign, Urbana, IL, USA. He was an Assistant Professor with the Department of Applied Mathematics and Statistics, University of California, Santa Cruz, CA, USA, from 2004 to 2007. He is currently a Professor in the Department of Mechanical and Aerospace Engineering, University of California, San Diego, CA, USA. He is the author of Geometric, Control and Numerical Aspects of Nonholonomic Systems (Springer-Verlag, 2002) and co-author (together with F. Bullo and S. Martínez) of Distributed Control of Robotic Networks (Princeton University Press, 2009). He has been an IEEE Control Systems Society Distinguished Lecturer (2010-2014) and is an elected member for 2018-2020 of the Board of Governors of the IEEE Control Systems Society. His current research interests include distributed control and optimization, network science, opportunistic state-triggered control and coordination, reasoning under uncertainty, and distributed decision making in power networks, robotics, and transportation.

Kameshwar Poolla is the Cadence Distinguished Professor at UC Berkeley in EECS and ME. His current research interests include many aspects of future energy systems including economics, security, and commercialization. He also serves as the Founding Director of the IMPACT Center for Integrated Circuit manufacturing. Dr. Poolla co-founded OnWafer Technologies which was acquired by KLA-Tencor in 2007. Dr. Poolla has been awarded a 1988 NSF Presidential Young Investigator Award, the 1993 Hugo Schuck Best Paper Prize, the 1994 Donald P. Eckman Award, the 1998 Distinguished Teaching Award of the University of California, the 2005 and 2007 IEEE Transactions on Semiconductor Manufacturing Best Paper Prizes, and the 2009 IEEE CSS Transition to Practice Award.